Test particles dynamics around deformed Reissner-Nordström black hole

Ashfaque Hussain Bokhari,[1,*] Javlon Rayimbaev,[2,3,†] and Bobomurat Ahmedov[2,3,4,‡]

[1]*Department of Mathematics and Statistics College of Science King Fahd University of Petroleum and Minerals (KFUPM), P.O. Box 31261, Dhahran 31262, Saudi Arabia*

[2]*Ulugh Beg Astronomical Institute, Astronomy St. 33, Tashkent 100052, Uzbekistan*

[3]*National University of Uzbekistan, Tashkent 100174, Uzbekistan*

[4]*Tashkent Institute of Irrigation and Agricultural Mechanization Engineers, Kori Niyoziy, 39, Tashkent 100000, Uzbekistan*

(Received 26 June 2020; accepted 13 December 2020; published 31 December 2020)

In this paper we study the dynamics of neutral, electrically charged and magnetized particles around deformed electrically and magnetically charged Reissner-Nordström black holes. For the neutral test particles motion, it is shown that the radius of the innermost stable circular orbits (ISCOs) decrease with the increase in both the black hole charge and positive spacetime deformation. It reaches up to $3.85M$ at the value of deformation parameter $\epsilon = 20.45$ in Schwarzschild spacetime case ($Q = 0$). In the extreme charged Reissner–Nordstrom black hole case, the ISCO decreases up to $2.26M$ at the value of deformation parameter $\epsilon = 6.17$. Moreover, the negative deformation results in an increase in the ISCO radius. Comparing effects of positive deformation and the Reissner-Nordström black hole charge with spin of rotating Kerr black holes, it is shown that the extremely charged Reissner-Nordström black hole can mimic rotating Kerr black hole up to the spin parameter $a/M = 0.48$, while for the positive deformation with $\epsilon = 6.17$ the mimic value increases up to $a/M = 0.88$ implying that the supermassive black hole M87 cannot be considered as Reissner-Nordström black hole. Using this comparison, we estimate charge of the supermassive black hole Sagittarius A* as $Q/M \simeq 0.8287$ without deformation which can mimic the spin of the black hole. When the deformation $\epsilon = 1$, the mimic charge increases up to $Q/M \simeq 0.8926$. Our study of the energy extraction from the accretion disk shows that the maximum energy efficiency increases up to 20.02%, which is almost the same for extreme Kerr black hole case (20.6%). We have also considered the behaviour of ISCO of electrically charged particles showing that the attractive (repulsive) electrostatic interactions cause rapid increase (slightly decrease) of the ISCO radius. Finally, we have explored the dynamics of magnetized particles around deformed magnetically charged Reissner-Nordström black hole. By treating the magnetar PSR J1745-2900, orbiting the supermassive black hole Sagittarius A* as a magnetized particle, showing that the magnetic charge of pure Reissner-Nordström black hole can mimic spin of a rotating Kerr black hole up to $a/M \simeq 0.82$ for the value to be in the range $Q_m/M \in (0, 0.692)$. Moreover, we find that the positive values of the deformation parameter lead to shift the ISCO for the magnetized particles toward the central object.

DOI: 10.1103/PhysRevD.102.124078

I. INTRODUCTION

The Einstein filed equations encode the spacetime physics through a system of highly nonlinear coupled partial differential equations. Due to their nonlinearity, these equations are extremely difficult to find their exact analytic solutions in terms of the gravitational potential. However, soon after their discovery, two very interesting exact solutions of these equation were obtained by Schwarzschild in 1916 and Reissner and Nordström in 1916 and 1918, respectively. These solutions respectively define the fields of a nonrotating neutral pointlike massive object [spherical symmetric black hole (BH)] and an electrically and magnetically charged nonrotating BHs in the framework of the linear electrodynamics for the electric field of BH generated by its net electric charge [1,2].

Whereas analytic static BH solutions have physical unavoidable singularity with the infinite spacetime curvature at the center of the BH ($r = 0$), it cannot be meaningfully explained within the context of classical theory of GR because of its being not quantum. It is worth mentioning that there exist so-called regular BH solutions for electrically and magnetically charged BHs, which avoid the singularity, in the framework of GR coupled to the nonlinear electrodynamics discussed by numerous authors in literature e.g., [3–7].

*abokhari@kfupm.edu.sa
†javlon@astrin.uz
‡ahmedov@astrin.uz

On the other hand, the accelerated expansion of the Universe and the discovery of the new forms of matter such as so-called dark matter and dark energy, led to the initiation of the development of alternate theories of gravity. It is expected that this study when applied to relativistic cosmology and astrophysics, one may find an explanation of the above mentioned unexpected phenomena not predicted by the standard cosmological models and solving the singularity problems in the gravitational field theory.

In addition, one may use another alternate approach to find a reasonable spacetime metric perturbing the exact analytical solution obtained in GR. Then a perturbation parameter can be expressed through a series of infinitesimally small expansion parameter and this approach can be termed as the phenomenological parameterization of the spacetime [8–11]. The detailed properties of the perturbed spacetime developed by Johannsen and Psaltis in Ref. [9] have been widely studied by number of authors in various aspects of relativistic astrophysics of gravitational compact objects [12–20].

The main issue with the alternate and modified theories is that they provide predictions similar to those as by GR in weak gravitational field regime, where it is well tested and the measurable discrepancies are enhanced as gravity becomes strong. Consequently, one of the main goals of the modern relativistic astrophysics is to test the validity of the GR with respect to alternate theories of gravity using observational data in the vicinity of BHs obtained in the strong gravitational field regime. Fortunately, recent triumphal discovery of the gravitational waves by LIGO-VIRGO collaboration [21–23], the detection of the first image of M87 supermassive BH by EHT collaborations [24,25], precise observation of the dynamics in supermassive black hole (SMBH) Sagittarius A* (Sgr A*) and M87 close environment by GRAVITY [26,27] team based on the advanced generation of observational facilities provide real opportunity to test extremely strong gravitational fields in the close BH environment with the most extreme gravitational field that can be found in the Universe. This can serve as ideal laboratories for testing the theories of gravity in the strong field regime [28]. Since BH environment is in the strong gravity regime, it may give a crucial key for testing gravity theories taking into account a possible degeneracy between effects of different parameters due to the indirect measurement of BH main parameters as a total mass and spin.

It is obvious that the properties of a spacetime can be studied considering the particle motion and their stability near the event horizon of BHs. The Spacetime properties, neutral and electrically and magnetically charged particles motion around electrically and magnetically charged Reissner-Nordström and regular BHs has been widely studied in [29–44]. From an astrophysical point of view, it is interesting to study the motion of charged particles around magnetized/charged BHs immersed in the external magnetic field. The motion of charged [45–54], magnetized [55–64] and spinning [65–68] particles around BHs with different parameters in an external asymptotically uniform magnetic field in various theories of gravity have recently been studied. While interpreting observations of the hot spots [69,70] and S-stars motion around SMBH Sgr A* [71], there is a degeneracy between the prediction made on the assumption that either the SMBH is rotating or some other type [31,46,72–78].

In this paper, we explore the dynamics of test particles around a deformed RN BH. In Sec. II we present a study of the motion of test particles around deformed charged RN BH. In Sec. III, we discuss motion of charged particles around electrically charged deformed RN BH. Magnetized particle dynamics around a deformed magnetically charged RN BH is explored in Sec. IV. We summarize main results in the last section.

Throughout this work we use the signature $(-,+,+,+)$ for the spacetime metric and geometrized unit system $G = c = 1$ (However, for an astrophysical application we will use the speed of light explicitly). Latin indices run from 1 to 3, while Greek ones take values from 0 to 3.

II. TEST PARTICLE MOTION

The geometry of the spacetime metric around deformed electrically and magnetically charged RN BH, in spherical polar coordinates, ($x^\alpha = \{t, r, \theta, \phi\}$) is given in the following [78] form:

$$ds^2 = -f(1+h)dt^2 + (1+h)f^{-1}dr^2 + r^2[d\theta^2 + \sin^2\theta d\phi^2], \tag{1}$$

with the following gravitational radially dependent RN metric function,

$$f = 1 - \frac{2M}{r} + \frac{Q^2 + Q_m^2}{r^2}. \tag{2}$$

Associated with the four vector potential in the above expression for the electromagnetic field around the deformed electrically and magnetically charged RN BH

$$A_\alpha = \left(-\frac{Q}{r}, 0, 0, Q_m \cos\theta\right), \tag{3}$$

where M is the total mass of the BH, Q and Q_m are the total electric and magnetic charges, respectively, and the radial function

$$h = \sum_{k=1}^{\infty} \epsilon_k \left(\frac{M}{r}\right)^k \tag{4}$$

is small dimensionless perturbation parameter. Due to its smallness $\epsilon_0 = 0$ ($\epsilon_0 \ll 1$), and similarly $\epsilon_1 \ll M/r$ and

$\epsilon_2 \simeq 4.6 \times 10^{-6}$ (as obtained using the observational data of Laser Lunar Ranging experiment (see for details [79]) are also extremely small. The lowest order nonvanishing parameter $\epsilon_3 = \epsilon$ called the deformation parameter, which can be either positive and/or negative describing oblate and prolate deformations respectively, and $k = 3$ (see for details [9]).

A. Equations of motion

In fact for study of neutral particles motion magnetic and electric charges of the RN BH are equivalent. Due to this reason, we will call these solutions as charged RN BH. Conservative quantities of the motion can be easily found by using the Euler Lagrange equation. The Lagrangian density for a neutral particle with mass m is,

$$\mathcal{L}_p = \frac{1}{2} g_{\mu\nu} \dot{x}^\mu \dot{x}^\nu, \tag{5}$$

and the conserved quantities of motion read

$$-E = p_t = \frac{\partial \mathcal{L}_p}{\partial \dot{t}}, \qquad \dot{t} = \frac{\mathcal{E}}{f(1+h)}, \tag{6}$$

$$L = p_\phi = \frac{\partial \mathcal{L}_p}{\partial \dot{\phi}}, \qquad \dot{\phi} = \frac{\mathcal{L}}{r^2 \sin^2\theta}, \tag{7}$$

where $\mathcal{E}$ represents energy and, $\mathcal{L}$ is the angular momentum of the particle. Equations of motion for a test particle in the equatorial plane are then governed by the normalization condition

$$g_{\mu\nu} u^\mu u^\nu = \kappa, \tag{8}$$

where κ 0 and -1 for massless and massive particles, respectively.

For the massive electrically uncharged particles the motion is governed by timelike geodesics of the spacetime, and the equations of motion can be found by using Eq. (8). Taking into consideration Eqs. (6)–(7), we obtain the equations of motion in the separated and integrated form as

$$(1+h)^2 \dot{r}^2 = \mathcal{E}^2 - f(1+h)\left(1 + \frac{\mathcal{K}}{r^2}\right), \tag{9}$$

$$\dot{\theta} = \frac{1}{g_{\theta\theta}^2}\left(\mathcal{K} - \frac{\mathcal{L}^2}{\sin^2\theta}\right), \tag{10}$$

where $\mathcal{K}$ denotes the Carter constant corresponding to the total angular momentum.

Restricting motion of the particle to the plane, in which $\theta = \text{const}$ and $\dot{\theta} = 0$, the Carter constant takes the form $\mathcal{K} = \mathcal{L}^2/\sin^2\theta$ and the equation of the radial motion can be expressed in the form,

$$(1+h)^2 \dot{r}^2 = \mathcal{E}^2 - V_{\text{eff}}, \tag{11}$$

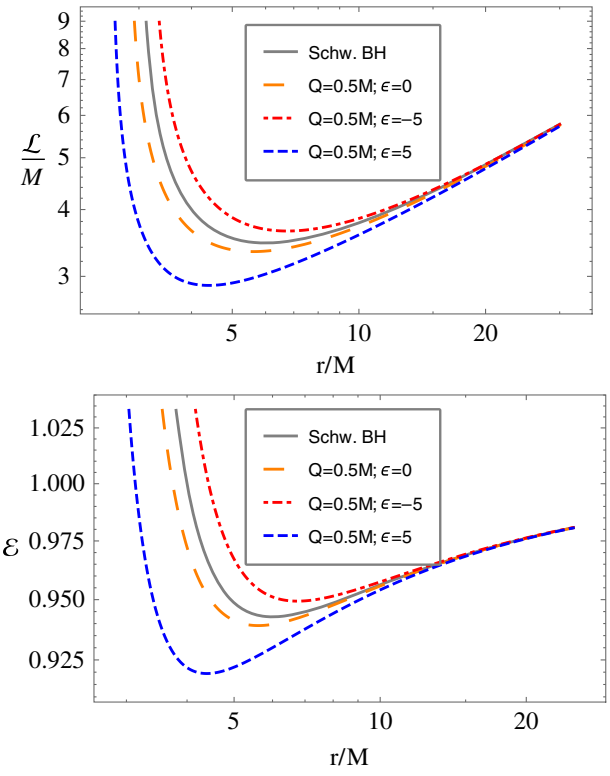

FIG. 1. The radial dependence of specific angular momentum (top panel) and energy (bottom panel) of the test particle in circular orbits for the different values of RN BH charge and spacetime deformation in comparison with Schwarzschild spacetime.

where it can be noted that the term $(1+h)^2$ in front of radial velocity $\dot{r}$ can be interpreted as the effective mass of the particles as $m_{\text{eff}} = m(1+h)^2$ and the effective potential of the motion of neutral particles reads

$$V_{\text{eff}} = f(1+h)\left(1 + \frac{\mathcal{L}^2}{r^2 \sin^2\theta}\right). \tag{12}$$

Now applying standard conditions for the circular motion, namely no radial motion ($\dot{r} = 0$) and no forces in the radial direction $\ddot{r} = 0$) we obtain the radial profiles of the specific angular momentum and specific energy for circular orbits at the equatorial plane ($\theta = \pi/2$) in the following form:

$$\mathcal{L}^2 = \frac{M^3 r^2 \epsilon[r(8M-3r) - 5Q^2] + 2r^5(Mr - Q^2)}{\mathcal{Z}},$$
$$\mathcal{E} = \frac{\sqrt{2}[r(r-2M) + Q^2](M^3\epsilon + r^3)}{r^2\sqrt{r\mathcal{Z}}}, \tag{13}$$

where

$$\mathcal{Z} = M^3\epsilon[r(5r-12M) + 7Q^2] + 2r^3[r(r-3M) + 2Q^2].$$

Figure 1 demonstrates radial profiles of specific and angular momentum of test particles around deformed RN

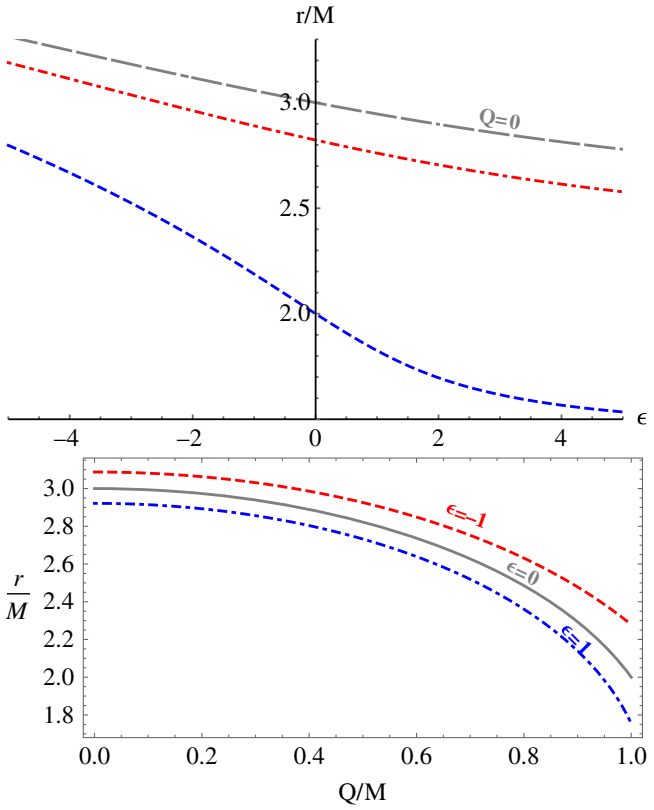

FIG. 2. The dependence of minimal distance where circular motion is allowed on RN BH charge (top panel) and spacetime deformation (bottom panel).

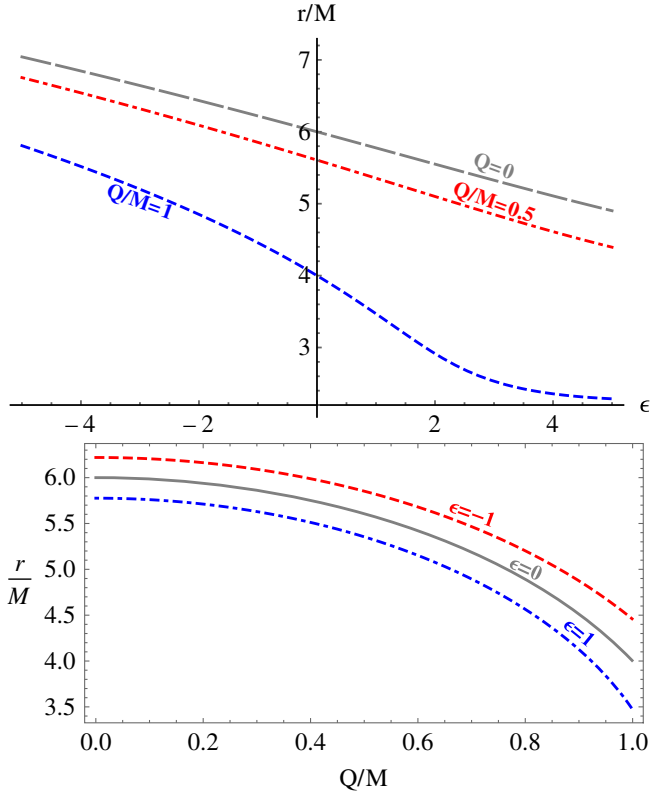

FIG. 3. The dependence of ISCO radius of test particles around deformed electrically charged RN BH from the BH charge (bottom panel) and spacetime deformation (top panel).

BH which correspond to circular orbits for the different values of deformation parameter at the fixed values of the BH charge with the comparison to the Schwarzschild case. One can see that existence of BH charge causes to decrease minimum values of both specific energy and angular momentum and the minimum value increases (decreases) with increasing the value of negative (positive) deformation.

From the expressions in Eq. (13), it can be seen that the circular orbits are bounded by the distance from the inside which are determined by $\mathcal{Z} = 0$,

Figure 2 demonstrates minimal distance for circular orbits of test particles as a function of deformation parameter (top panel) and the BH charge (bottom panel). One can see that the increase of both deformation parameter and charge of the RN BH causes to decrease of the radius. Moreover, the minimum radius is more sensitive to the variation of the deformation parameter near extreme value of the BH charge.

B. Innermost stable circular orbits–ISCO

Traditionally, the stable circular orbits equation is defined by the standard condition $\partial_{rr}V \geq 0$ and ISCO corresponds to the case when $\partial_{rr}V = 0$. In this context the equation for the ISCO radius of neutral particles in the spacetime (1) takes the following form: w

$$
\begin{aligned}
&2M^6\epsilon^2[r^2(96M^2 - 74Mr + 15r^2) + 35Q^4 \\
&\quad + 6Q^2r(7r - 19M)] - 2M^3r^3\epsilon[60MQ^2r \\
&\quad - 6r^2(6M^2 + Q^2) + 4Mr^3 - 25Q^4 + 3r^4] \\
&\quad - 4r^6(9MQ^2r + Mr^2(r - 6M) - 4Q^4) = 0. \qquad (14)
\end{aligned}
$$

It is quite hard to solve Eq. (14) with respect to the radial coordinate which corresponds to ISCO radius. For this reason we try to analyze the behaviour of ISCO radius numerically which can provide the dependence of ISCO radius from electric charge of the deformed RN balck hole (bottom panel) and deformation parameter (top panel).

One can see from Fig. 3 that deformation parameter and the RN BH charge are responsible in decrease of ISCO radius. Moreover, the effect of deformation parameter become much stronger when the BH charge reaches its extreme value.

Assume consider deformation parameter is a free parameter and ISCO radius as a function of it for the fixed values of the BH charge

In Fig. 4 we provide ISCO radius behaviour on the variable deformation parameter for the Schwarzschild and extreme charged RN BH. One may see that ISCO radius has a minimum value at some value of deformation parameter depending on BH charge between $\epsilon \in (6.17411 \div 20.4547)$

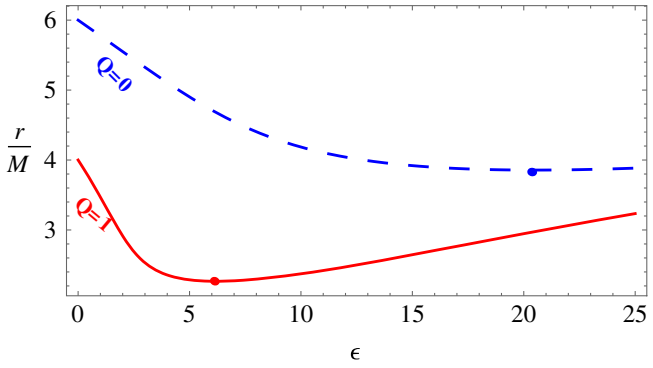

FIG. 4. The dependence of ISCO radius from deformation parameter for the fixed values of the BH charge.

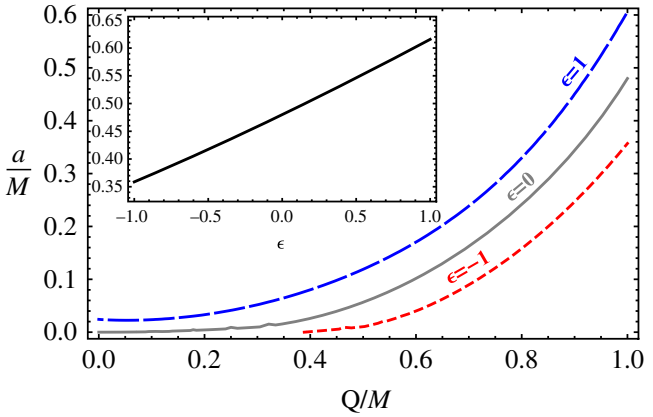

FIG. 5. Relationship between spin of rotating Kerr BH and charge of RN BH for the different values of deformation parameter providing the same values for ISCO radius of test particles.

for the range of BH charge $Q \in (1, 0)$, respectively, giving minimuma for ISCO radius $(r_{\rm isco})_{\rm min} \in (2.2665, 3.8564)M$.

C. Deformed RN BH versus Kerr BH: Degeneracy providing the same ISCO radius

Here we will carry out testing the spacetime strong gravity effects of deformed RN BH on ISCO in real astrophysical (direct and/or indirect) observations of ISCO radius. Since positive deformation parameter and the BH charge cause decrease of ISCO radius, on the other hand spin of Kerr BH in prograte orbits also provides similar effect. Due to the degeneracy, from observational point of view, in these cases it is hard to distinguish the type of BHs. Here we will carry out detail analysis to distinguish the effects of spacetime deformation and BH charge from spin of the Kerr BH.

The well-known expression for ISCO radius of the test particles at retrograde and prograde orbits around rotating Kerr BH is [80],

$$r_{\rm isco} = 3 + Z_2 \pm \sqrt{(3 - Z_1)(3 + Z_1 + 2Z_2)}, \quad (15)$$

where the following notations are used

$$Z_1 = 1 + (\sqrt[3]{1+a} + \sqrt[3]{1-a})\sqrt[3]{1-a^2},$$
$$Z_2^2 = 3a^2 + Z_1^2.$$

Here, we will provide a comparison of the effects of spacetime deformation, electric charge of the deformed RN BH and spin of rotating Kerr BHs on the ISCO radius.

Figure 5 illustrates degeneracy values of the BH charge and spin parameters providing the same ISCO radius. One can see from the figure that the electric charge of non-deformed RN BH can mimic spin of rotating Kerr BH up to $a/M = 0.479875$, and for positive (negative) deformation the mimic value increases (decrease). For the estimation the realistic case in which value of charge of RN SMBH Srg A* can mimic it is obtained spin parameter at $\epsilon = 0$ charge of SgrA* $10^3 Q/M = 828.71^{+70.58}_{-60.94}$ [31] and at $\epsilon = 1$ it is $10^3 Q/M = 892.68^{+64.62}_{-55.20}$, however the negative deformation of the BH cannot mimic the spin of the SMBH SgrA*. Authors of Ref. [81,82] estimate an upper limit for electric charge of the SMBH SgrA* in order of $\approx 10^{15} C$.

Analysis of ISCO radius at $Q/M = 1$ shows that extreme charged deformed RN BH can mimic spin of rotating Kerr BH up to $a/M = 0.881399$. This confirms once again that the SMBH M87 BH cannot be RN BH even the BH is extremely charged.

Figure 6 illustrates relationship between negative deformation parameter and spin parameters giving the same counter-rotating innermost orbits. One may see that spin parameter can mimic the negative deformation in the range of $\epsilon = -16.9535$ for the non-Schwarzschild BH case when $Q = 0$, and in the extremely charged RN BH case the spin parameter cam mimic in the range of $\epsilon \in (-21.8525, -5.7133)$.

D. The energy efficiency

An other interesting issue arises when consider test particle in Keplerian accretion disk falls down to the central

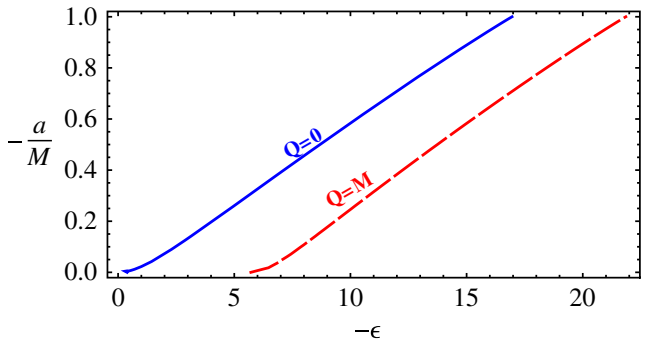

FIG. 6. Relations of degeneracy values of negative deformation and spin of Kerr BH providing the same value for innermost stable prograde orbits.

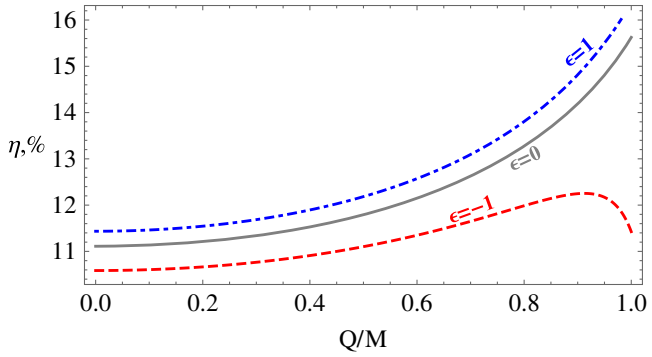

FIG. 7. Dependence of energy efficiency from the charge of RN BH for the different values of the parameter ϵ.

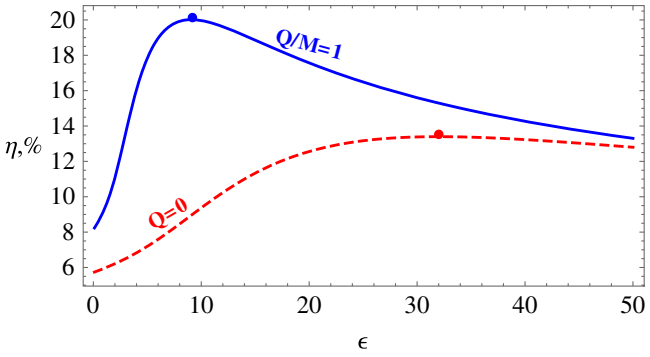

FIG. 8. Dependence of energy efficiency from the deformation parameter ϵ for the different values of the electric charge of RN BH.

BH and extracts energy which converted to (electromagnetic and/or gravitational) radiation(s). The radiated energy is determined by the difference of the rest energy of the particle measured by local observer and the energy of the particle at ISCO, which reflects spacetime properties. Consequently, the energy efficiency of accretion disk can be calculated through the following expression [83]

$$\eta = 1 - \mathcal{E}|_{r=r_{\rm ISCO}}, \tag{16}$$

where $\mathcal{E}_{\rm ISCO}$ is the energy of the particle at the ISCO which is characterized by ratio of the binding energy (BH- particle system) and rest energy of test particle.

The dependence of the energy efficiency from electric charge of RN BH for the different values of deformation parameter is shown in Fig. 7. One can see from the figure that energy efficiency from the accretion disk increases as the increase of electric charge of the BH. Moreover, the existence of positive (negative) deformation causes to increase (decrease) of the efficiency.

Now we are interested to calculate value of deformation parameter when the energy efficiency reaches its maximum value depending on the BH charge. As we know, the charge can be $|Q|/M \to [0, 1]$, therefore we will test the maximum of energy efficiency at this range of the BH charge. Assume that deformation parameter as a free parameter of the energy efficiency and one may find the critical deformation parameter which makes the energy efficiency maximum by solving the following equation numerically

$$\partial_\epsilon \eta(\epsilon, Q) = 0, \tag{17}$$

with respect to deformation parameter and substitute the critic deformation parameter calculated into $\eta(\epsilon, Q)$ for the given value of the BH charge Q.

Figure 8 shows dependence of energy efficiency from deformation parameter for the values of the BH electric charge $Q = 0$ and $Q = M$. One may see from Fig. 8 that the maximum value of the energy efficiency at $\epsilon = 32$ for non-Schwarzschild BH case $Q = 0$ provides maximum efficiency $\eta = 13.3975\%$ and when $\epsilon = 9.07407$ for the extremely charged RN BH case $Q/M = 1$ it provides maximum efficiency $\eta = 20.0167\%$. Since energy efficiency from extreme Kerr BHs is around 20.6%. In fact the bolometric luminosity of accretion disk brightness is proportional to the energy efficiency of the central BH through the relation $\eta = L_{\rm bol}/(\dot{M}c^2)$, where $\dot{M}$ is the accretion rate [84]. From this point of view one may conclude that extremely charged RN BH with the deformation parameter $\epsilon = 9.07407$ does is not distinguishable from the nearly extreme rotating Kerr BH providing the same total bolometric luminosity. For a rapidly rotating Kerr BH the inner edge of the accretion disk is considerably closer to the event horizon than for a Shwarzschild BH. For a maximally rotating BH, the inner edge can be as close as $1.2M$, while for the Schwarzschild ISCO radius is $6M$. This is 5 times closer than for a nonrotating black hole, and the velocities of the material can be ultrarelativistic in addition to a gravitational redshift from the central BH. Fitting of the spectrum and luminosity can indicate that the inner edge of the disk is at $\approx 2M$ and the high luminosity, but it cannot indicate exactly whether the BH is spinning quite rapidly or RN BH. More data can be used in order to rule out the alternate BH candidates [85–89]. X-ray missions such as XMM (Newton) and AXAF (Chandra) offer greatly increased sensitivity and would be able to map the luminosity and inner regions of accretion disks around black holes in detail.

III. MOTION OF ELECTRICALLY CHARGED PARTICLES AROUND DEFORMED ELECTRICALLY CHARGED RN BH

Here we will study of electrically charged particles motion around deformed electrically charged RN BH with e as electric charge of the particle. The Lagrangian for electrically charged particles in electromagnetic fields has the following form:

$$\mathcal{L} = \frac{1}{2} m g_{\mu\nu} u^\mu u^\nu + e u^\mu A_\mu. \tag{18}$$

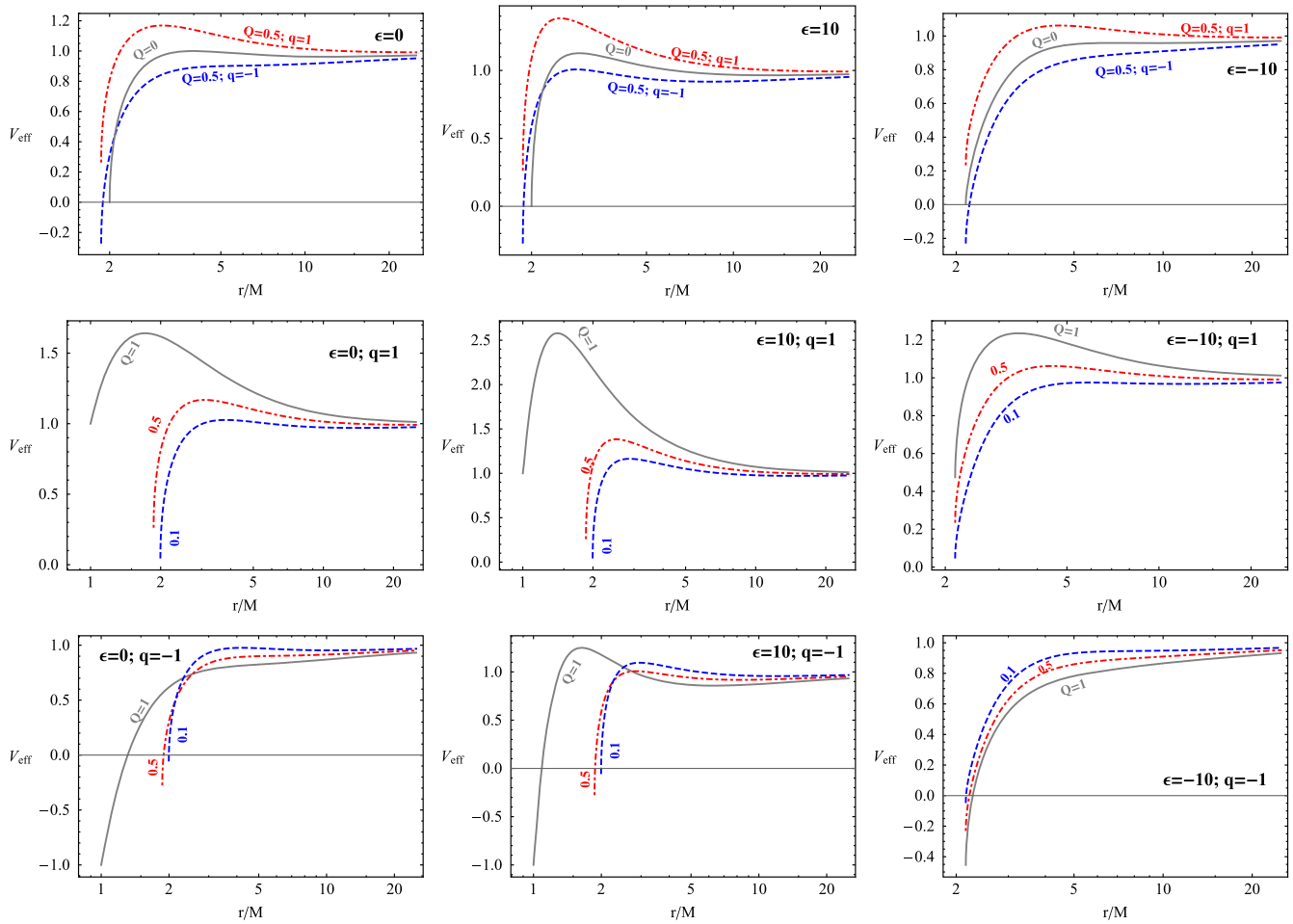

FIG. 9. Effective potential analysis for the radial motion of electrically charged particles around deformed electrically charged RN BH for the different values of deformation parameter, charge of the BH and the particle.

For the case of deformed electrically charged RN BH the specific angular momentum is exactly the same as neutral particle's angular momentum. However, the specific energy is different from neutral particle's energy due to existence of A_t and it can be obtained by,

$$g_{tt}\dot{t} + qA_t = -\mathcal{E}, \tag{19}$$

where "dot" represents derivative with respect to proper time, $q = e/(mc)$ is the specific electric charge of the particle and electric charge e.

One can find the equation of motion for electrically charged particles with the Lagrangian (18) using the Euler-Lagrange equations [29],

$$u^\mu \nabla_\mu u^\nu = qF^\nu_\sigma u^\sigma, \tag{20}$$

where $F^\nu_\sigma = g^{\mu\nu}F_{\mu\sigma}$ and $F_{\mu\sigma} = A_{\sigma,\mu} - A_{\mu,\sigma}$ is the electromagnetic field tensor. Using the Eqs. (19)–(20), one may easily find the equation of motion of the charged particles in the equatorial plane ($\theta = \pi/2$) in the following form:

$$\dot{t} = \frac{1}{f(1+h)}\left(\mathcal{E} - \frac{qQ}{r}\right), \tag{21}$$

$$(1+h)^2\dot{r}^2 = \left(\mathcal{E} - \frac{qQ}{r}\right)^2 - f(1+h)\left(1 + \frac{\mathcal{L}^2}{r^2}\right). \tag{22}$$

The effective potential for charged particles in the equatorial plane (where $\theta = \pi/2$ and $\dot{\theta} = 0$) can be easily found by solving the equation $\dot{r} = 0$ in Eq. (22) with respect to the specific energy ($\mathcal{E} = V_{\text{eff}}$) and we have

$$V^{\pm}_{\text{eff}}(r) = \frac{qQ}{r} \pm \sqrt{f(1+h)\left(1 + \frac{\mathcal{L}^2}{r^2}\right)}. \tag{23}$$

In this study, we will investigate the positive root of the effective potential–V^+_{eff}, in Eq. (23), while the second solution is not interesting physically because:

(i) when, $|qQ/r| < \sqrt{f(1+h)(1+\mathcal{L}^2/r^2)}$ the second root of the effective potential V^-_{eff} is negative

(ii) when, $|qQ/r| > \sqrt{f(1+h)(1+\mathcal{L}^2/r^2)}$ the effective potential $V_{\rm eff}^-$ has neither maximum nor minimum.

Radial dependence of effective potential for radial motion of electrically charged particles around electrically charged RN BH for different values of deformation parameter, BH and particle charge shown are in Fig. 9. The left column corresponds to pure RN BH, middle and right correspond for the values of deformation parameter $\epsilon = 10$ and $\epsilon = -10$, respectively. The top row corresponds to the fixed value of the electric charge of the BH $Q = 0.5$ with comparison to the Schwarzschild hole for negatively and positively charged particles, middle and bottom rows correspond to positively and negatively charged particles, respectively. One can see from the figure (the first row from left to right) that the maximum of the effective potential increases (decreases) with the increase of positive (negative) deformation parameter and for the positively charged particles the maximum of the effective potential increases (decreases) with the increase of BH charge. However, for negatively charged particles, the maximum decreases (increases) in the cases of $\epsilon \leq 0$ ($\epsilon > 0$).

A. Stable circular orbits

In this subsection, we will focus our attention to the studies of stable circular orbits of electrically charged particles around deformed electrically charged RN BH at the equatorial plane through the following standard conditions:

$$V_{\rm eff} = \mathcal{E}, \qquad V'_{\rm eff} = 0, \qquad V'_{\rm eff} \geq 0. \tag{24}$$

The circular orbits can be stable for the critical value of angular momentum $\mathcal{L}_{\rm cr} \geq \mathcal{L}_{\rm min}$ which describes through the solution of the equation $V'_{\rm eff} = 0$ with respect to the specific angular momentum, and we have:

$$\begin{aligned}\mathcal{L}^2_{\pm} = {} & \{M^3\epsilon(r(5r-12M)+7Q^2)+2r^3(r(r-3M)+2Q^2)\}^{-2} \\ & \pm 2qQr^{7/2}[r(r-2M)+Q^2](M^3\epsilon+r^3)\sqrt{2M^3\epsilon[r(5r-12M)+7Q^2]+r^3[4r(r-3M)+(q^2+8)Q^2]} \\ & + 2q^2Q^2r^5[r(r-2M)+Q^2](M^3\epsilon+r^3)+r^2\{M^3\epsilon[r(8M-3r)-5Q^2]+2r^3(Mr-Q^2)\} \\ & \times\{M^3\epsilon[r(5r-12M)+7Q^2]+2r^3[r(r-3M)+2Q^2]\}.\end{aligned} \tag{25}$$

One can see from Eq. (25) that there are two positive real solution for the specific angular momentum and it is for positive qQ, $\mathcal{L}^2_+ < \mathcal{L}^2_-$ and for negative qQ, it is $\mathcal{L}^2_- > \mathcal{L}^2_+$. In other words, these two solutions are symmetric with respect to the substitution of the sign of qQ and this aspect of the symmetries describes the nature of Coulomb (repulsive and attractive) interaction in the specific angular momentum of electrically charged particles for circular orbits.

$$\mathcal{L}^2_+|_{qQ<0} = \mathcal{L}^2_-|_{qQ>0} < \mathcal{L}^2_+|_{qQ>0} = \mathcal{L}^2_-|_{qQ<0}. \tag{26}$$

Despite symmetries of the solutions Eq. (25), the condition given by Eq. (26) shows our hesitance to choose which solution is correct to study the electrically charged particles dynamics at the equatorial plane for circular stable orbits. In order for the choice of the solution to be correct, we simply discuss the dynamics of charged particles. Obviously that there are three forces acting on the charged particle around deformed electrically charged RN BH, (i) Coulomb, (ii) gravitational and (iii) centrifugal forces.

(i) Coulomb and gravitational forces are the same in direction for $qQ < 0$ attracting the particle into the central object, then centrifugal force balances the attractive forces when the orbit of the particle is stable and circular. In this case, we have to take bigger solutions using the definition in Eq. (26).
(ii) Coulomb and centrifugal forces play the same role compensating gravitational forces in the circular orbits. Thus, this requires smaller one from the definition Eq. (26).

This can be interpreted as follows: the circular orbits can exist at the values of angular momentum for positive qQ with angular momentum in the range $\mathcal{L}^2_- \leq \mathcal{L}^2 \leq \mathcal{L}^2_+$ and negative qQ with angular momentum in the range $\mathcal{L}^2_- \geq \mathcal{L}^2 \geq \mathcal{L}^2_+$. This implies that taking above into considerations, we will work with the positive solution of the critical specific angular momentum of electrically charged particle for circular motion in Eq. (25).

The value of critical angular momentum for electrically charged particles in the case of pure RN BH takes the form,

$$\begin{aligned}\mathcal{L}^2_{\pm} = {} & \frac{r^2}{2[r(r-3M)+2Q^2]^2}\left\{r^2\left(2M(r-3M)\pm\frac{qQ}{r^2}[r(r-2M)+Q^2]\sqrt{4r(r-3M)+(q^2+8)Q^2}\right)\right. \\ & \left. + Q^2r[(q^2-2)r-2M(q^2-5)]+(q^2-4)Q^4\right\},\end{aligned} \tag{27}$$

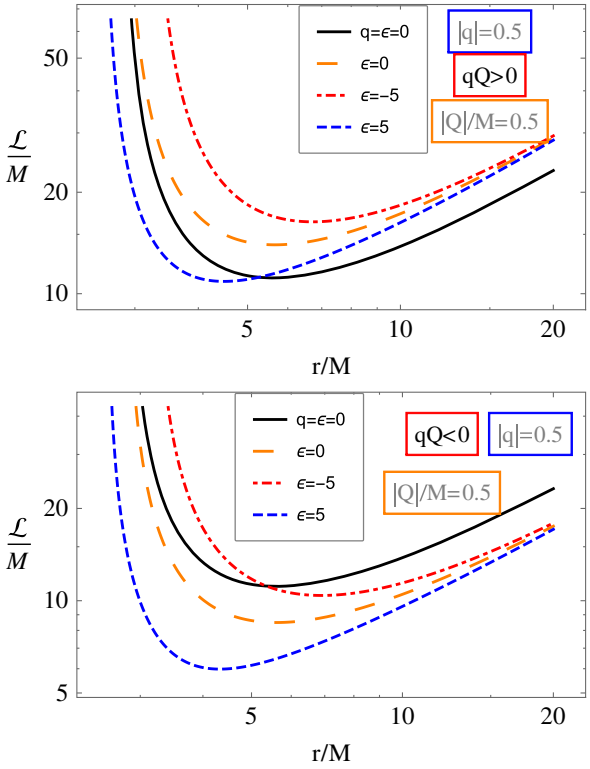

FIG. 10. The radial dependence of specific angular momentum and energy of positively (top panel) and negatively (bottom panel) charged particles in circular orbits for the different values of RN BH charge and spacetime deformation.

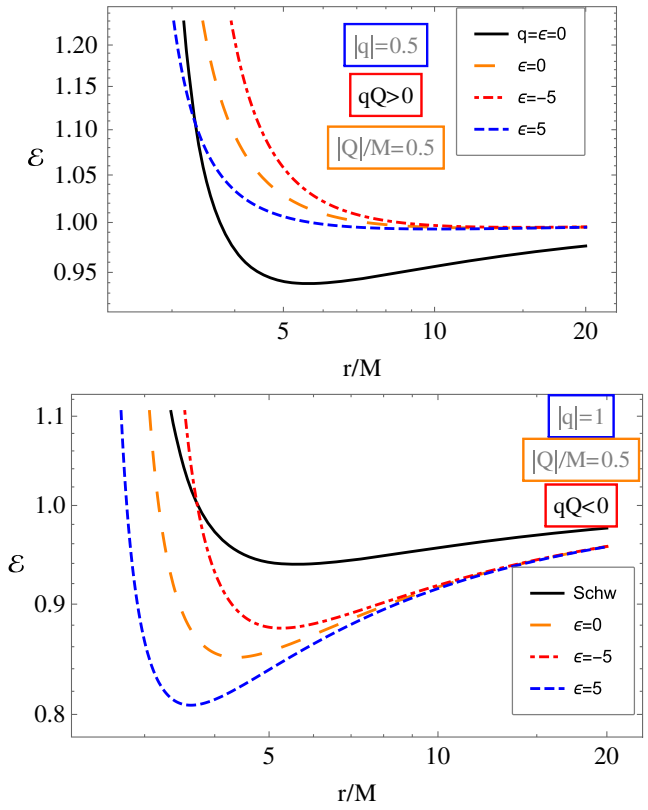

FIG. 11. The radial dependence of specific energy of positively (on the top panel) and negatively (on the bottom panel) charged particles in circular orbits for the different values of RN BH charge and spacetime deformation in comparison to the Schwarzschild spacetime.

and for neutral particles ($q = 0$) the form is given in Eq. (13) and $\epsilon = 0$ takes the following form:

$$\mathcal{L}_{\pm}^2 = \frac{r^2(Mr - Q^2)}{r(r - 3M) + 2Q^2},$$

At least in the Schwarzschild BH when $Q = 0$, the angular momentum takes the standard form

$$\mathcal{L}_{\pm}^2 = \frac{Mr^2}{r - 3M}.$$

Figure 10 illustrates radial dependence of specific angular momentum of charged particles around deformed electrically charged RN BH for the different values of deformation parameter. One may see that the minimum value for the specific angular momentum increases (decreases) for positive (negative) charges and the existence of positive (negative) deformation parameter causes to increase (decrease) of the specific angular momentum. However, it is quite difficult to observe the effect of charge of particle at the position where the specific angular momentum is minimum (which corresponds to ISCO). Thus we will study the effects of particle's charge effects on the ISCO radius in detail in the next section together with the spacetime deformation.

Radial profiles of specific energy of charged particles around deformed electrically charged RN BH for the different values of deformation parameter shown are in Fig. 11. One can see from the figure that the energy increases (decreases) with the increase of positively (negatively) charged particles due to negative Coulomb interaction.

Now we will analyze the condition which make $\mathcal{L}_{\pm}^2$ real. For this, we require the part inside the square root in Eq. (25) to be always non-negative:

$$2M^3\epsilon[r(5r - 12M) + 7Q^2] + r^3[4r(r - 3M) + (q^2 + 8)Q^2] \geq 0. \quad (28)$$

At the same time condition given in Eq. (28) also ensures that the denominator of Eq. (25) should not be zero. One may see that it is impossible to solve Eq. (28) with respect to the radial coordinate. One way to see the effect of spacetime deformation and charge of particle on minimum radius for circular orbits is to solve it numerically and show in plot form.

Figure 12 illustrates the dependence of minimum radius for circular orbits of electrically charged particles around

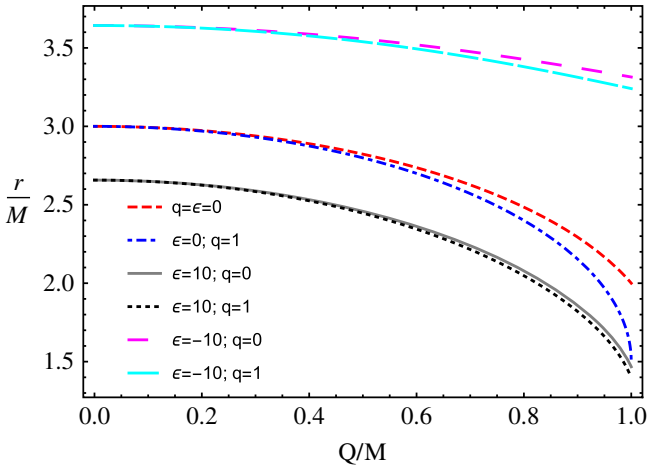

FIG. 12. The dependence of minimal distance where circular motion is allowed from RN BH charge and spacetime deformation.

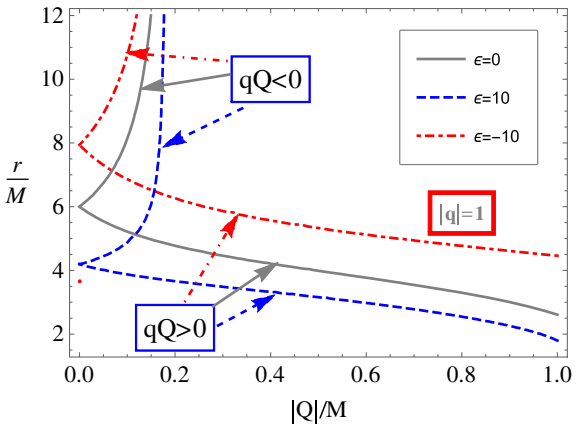

FIG. 13. Dependence of ISCO radius of electrically charged particle with the specific charge $q = \pm 1$ (top and bottom panels, respectively) from the electric charge of BH Q/M for the different values of deformation parameter.

deformed RN BH from charge of the BH for the different values of particle's charge and spacetime deformation. One can see that the minimum value for radius of circular orbits increases (decreases) on the existence of negative (positive) deformation and the effects of particle's charge on the radius is reasonable near the extreme value of the BH charge and it is very sensitive for pure RN BH spacetime.

The solution of Eq. (28) with respect to the radial coordinate provides the lower value for radius of the circular orbit of particle when $\mathcal{L}$ is still real at $\epsilon = 0$. Fortunately, it is possible to get analytic expression for minimal radius for circular orbits in the following form:

$$r_{\rm crit} = \frac{3}{2}M\left(1 + \sqrt{1 - \frac{q^2+8}{9}\frac{Q^2}{M^2}}\right). \tag{29}$$

Again, in order to have real value for $r_{\rm crit}$, we require the expression under the square root in expression (29) to be non-negative: $9M^2 - (q^2+8)Q^2 \geq 0$. This provides range of values for particles charge which allows them to be in circular orbits. This implies that particles with the values out of the range cannot be in circular orbits due to higher Coulomb interaction:

$$-\sqrt{9M^2/Q^2 - 8} \leq q \leq \sqrt{9M^2/Q^2 - 8}. \tag{30}$$

Expression (30) indicates the allowed value of the charge of the test particle required for circular stable orbits.

Now we will investigate the radius of ISCOs using the condition $V''_{\rm eff} \geq 0$. Obviously, the ISCO radius behavior strongly depends on the Coulomb interaction (the sign of qQ) and spacetime deformation. Therefore, we will study the ISCO radius of electrically charged particles with the specific electric charge $q = 1$ for cases $qQ > 0$ and $qQ < 0$.

In Fig. 13 we demonstrate dependence of ISCO radius of (positively and negatively) charged particles around deformed RN BH from electric (positive and negative) charge of the BH for different values of deformation parameter. One can see that ISCO radius is rapidly increased with the increase of the BH charge when the sign of qQ is positive (decreased) due to attractive nature of Coulomb interaction. Thus, ISCO radius goes outward from (comes close to) the central object where the forces acting on the charged particle are balanced. Moreover, the existence of negative (positive) deformation causes increase (decrease) of ISCO radius for the fixed values of the BH and particle charge. We have tested the effects of spacetime deformation on ISCO radius of electrically charged particle in Fig. 13 in the fixed values of the deformation parameter. However, in order to see/understand deeply the effects of spacetime deformation we will consider the parameter as a free parameter of the ISCO radius.

The dependence of ISCO radius of electrically charged particles with specific charge parameter $q = \pm 1$ from deformation parameter for positive and negative signs of qQ (repulsive and attractive Coulomb force, in the top and bottom panels, respectively) at different values of the BH charge is presented in Fig. 14. One can see from the figures that in both cases the increase of negative (positive) deformation parameter causes increase of the ISCO radius and the effect of negative deformation is more stronger than the effect of positive one, especially when it becomes more stronger at larger values of the BH charge.

We will now analyze both electric charge of the BH and spacetime deformation effects on ISCO radius for the cases when sign of qQ is positive and negative.

Figure 15 demonstrates relations between spacetime deformation and RN BH charge providing different values of ISCO radius of the charged particle with the specific electric charge $q = \pm 1$ for attractive and repulsive

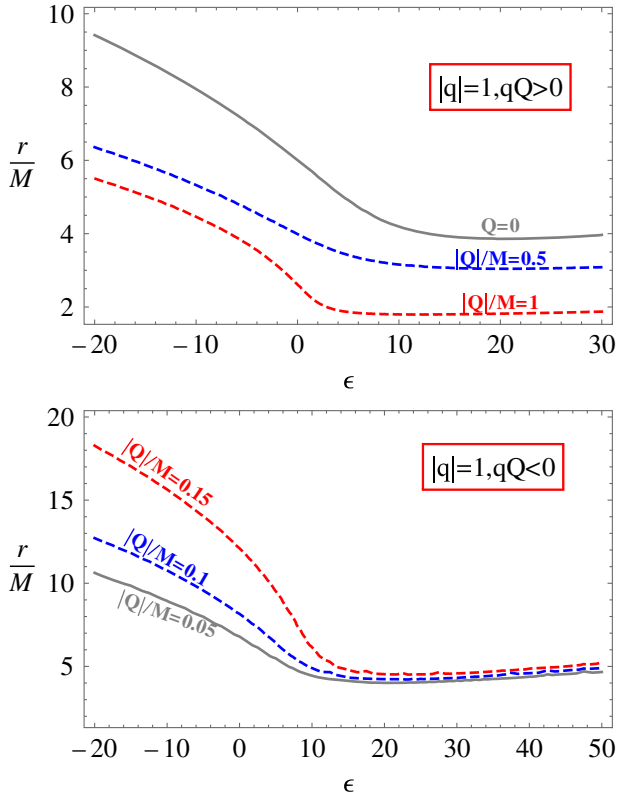

FIG. 14. Dependence of ISCO radius of electrically charged particle with the specific charge $q = \pm 1$ from deformation parameter for the different values of the electric charge of BH Q/M.

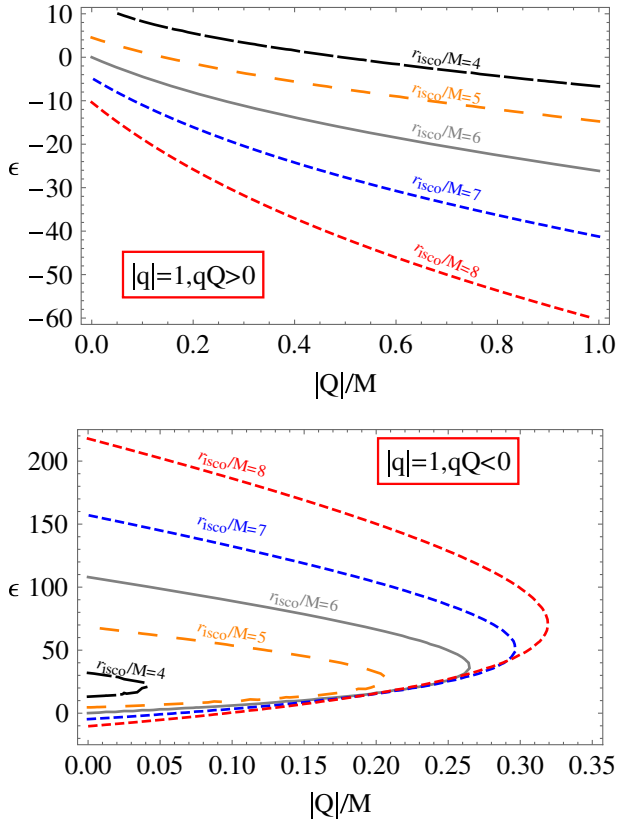

FIG. 15. Relations between deformation parameter and electrically charge of RN BH with the specific charge $|q| = 1$ (top and bottom panels, respectively) for different values of ISCO radius.

Coulomb interaction, at bottom and top panels, respectively. One can see from the figures that when $qQ > 0$ $(qQ < 0)$ in order for the charged particle to stay in the same ISCO deformation parameter has to be increased (decreased) with the increase of BH charge. Moreover, in case when qQ is negative there are two degeneracy values for deformation parameter at $Q < Q_{\rm crit}$ for a given values of ISCO radius. One may explain this that since electrostatic interaction does not change the increase of spacetime deformation it, causes increase of the specific angular momentum giving additional gravitational attractive effects.

IV. MAGNETIZED PARTICLES MOTION AROUND DEFORMED MAGNETICALLY CHARGED RN BH

In this section, we explore the motion of magnetized particles around the deformed magnetically charged RN BH. The nonvanishing component of the electromagnetic field tensor can be found using 4-potential provided in Eq. (3) in the following form:

$$F_{\theta\phi} = -Q_m \sin\theta. \tag{31}$$

From this nonzero component of the electromagnetic field tensor, one can easily obtain component of the magnetic field generated by magnetic charge of the deformed RN BH measured by zero angular momentum observer (ZAMO) by the following relations

$$B^{\alpha} = \frac{1}{2}\eta^{\alpha\beta\sigma\mu}F_{\beta\sigma}w_{\mu}, \tag{32}$$

where w_{μ} is four-velocity of the proper observer, $\eta_{\alpha\beta\sigma\gamma}$ is the pseudotensorial form of the Levi-Civita symbol $\epsilon_{\alpha\beta\sigma\gamma}$ with the relations

$$\eta_{\alpha\beta\sigma\gamma} = \sqrt{-g}\epsilon_{\alpha\beta\sigma\gamma} \qquad \eta^{\alpha\beta\sigma\gamma} = -\frac{1}{\sqrt{-g}}\epsilon^{\alpha\beta\sigma\gamma}, \tag{33}$$

and $g = \det|g_{\mu\nu}| = -(1+h)r^2\sin^2\theta$ for spacetime metric (1). Thus, the orthonormal radial component of the magnetic field is

$$B^{\hat{r}} = \frac{Q_m}{r^2}. \tag{34}$$

One can easily see from Eq. (34) that the radial component of the magnetic field around the deformed magnetically charged BH does not reflect the effects of the spacetime

gemetry (1) and formally looks like an expression in the Newtonian framework.

Equation of motion of magnetized particles in the spacetime exterior to the magnetically charged BH can be described by the Hamilton-Jacobi equation, first formulated by de-Felice in Ref. [55]

$$g^{\mu\nu}\frac{\partial\mathcal{S}}{\partial x^{\mu}}\frac{\partial\mathcal{S}}{\partial x^{\nu}}=-\left(m-\frac{1}{2}D^{\mu\nu}F_{\mu\nu}\right)^{2}, \tag{35}$$

where the product of the polarization and electromagnetic field tensors $D^{\mu\nu}F_{\mu\nu}$ stands for the interaction between the magnetic field generated by the magnetic charge of the BH and dipole moment of the magnetized particle. Here, the polarization tensor $D^{\mu\nu}$ corresponds to the magnetic dipole moment of the magnetized particle and it can be described by the relation [55]:

$$D^{\alpha\beta}=\eta^{\alpha\beta\sigma\nu}u_{\sigma}w_{\nu},\qquad D^{\alpha\beta}w_{\beta}=0, \tag{36}$$

where μ^{ν} is the four-vector of the magnetic dipole moment measured by the proper observer. The electromagnetic field tensor has the following form:

$$F_{\alpha\beta}=w_{[\alpha}E_{\beta]}-\eta_{\alpha\beta\sigma\gamma}w^{\sigma}B^{\gamma}. \tag{37}$$

The product of polarization and electromagnetic tensors in Eq. (35) can be obtained using Eq. (36) in the following form:

$$D^{\mu\nu}F_{\mu\nu}=2\mu^{\hat{\alpha}}B_{\hat{\alpha}}, \tag{38}$$

where $\mu=\sqrt{\mu_{\hat{i}}\mu^{\hat{i}}}$ is the norm of the dipole magnetic moment of magnetized particles measured also by the proper observer.

In the case when the direction of the external magnetic field coincides with that of the magnetic dipole moment of the magnetized particles, the magnetic interaction will be in the equilibrium state with the minimum energy. In order to provide the magnetized particle a stable equilibrium, we assume that the magnetic dipole moment direction is the same as that of the magnetic field generated by the magnetic charge of the deformed RN BH being parallel to the equatorial plane and has the following orthonormal components: $\mu^{\hat{i}}=(\mu^{\hat{r}},0,0)$.

Moreover, the second part of the condition (36) allows one to study the particle motion in the ZAMO frame and the choice of the observer velocity may help to avoid a relative motion problem. The magnitude of the magnetic moment is constant and maintained during the motion. One may therefore rewrite the interaction term of the Homilton-Jacobi equation given in Eq. (35) using Eqs. (38) and (31) in the following form:

$$\mathcal{D}^{\alpha\beta}F_{\alpha\beta}=\frac{2\mu Q_{m}}{r^{2}}. \tag{39}$$

Now, one can investigate the radial motion of magnetized particles around the deformed magnetically charged RN BHs at the equatorial plane using Eqs. (35) and (39)

$$(1+h)^{2}\dot{r}^{2}=\mathcal{E}^{2}-V_{\rm eff}(r;l,\mathcal{B}). \tag{40}$$

The effective potential for the radial motion has the following form:

$$V_{\rm eff}(r;l,\mathcal{B},Q_{m})=\left(1-\frac{2M}{r}+\frac{Q_{m}^{2}}{r^{2}}\right)\left(1+\epsilon\frac{M^{3}}{r^{3}}\right)\times\left[\left(1-\frac{\mathcal{B}}{r^{2}}\right)^{2}+\frac{\mathcal{L}^{2}}{r^{2}}\right]. \tag{41}$$

Here we introduce the relation $\mathcal{B}=\mu Q_{m}/m$ being responsible for the interaction between dipole magnetic moment of the magnetized particles and the proper magnetic field created by magnetic charge of the deformed RN BH. For the qualitative analysis, we introduce another new parameter $\beta=\mu/(mM)$ which characterizes properties of the magnetized particle and the central BH which is always positive. In real astrophysical scenario, when magnetized neutron star treated as a test magnetized particle orbiting around a SM BH, the parameter β can be described as

$$\beta=\frac{B_{\rm NS}R_{\rm NS}^{3}}{2m_{\rm NS}M_{\rm SMBH}}\simeq 0.034\left(\frac{B_{\rm NS}}{10^{12}\ \rm G}\right)\left(\frac{R_{\rm NS}}{10^{6}\ \rm cm}\right)\left(\frac{m_{\rm NS}}{1.4\times M_{\odot}}\right)^{-1}\times\left(\frac{M_{\rm SMBH}}{3.8\times 10^{6}\ M_{\odot}}\right)^{-1}. \tag{42}$$

For example, the value of the parameter β for the magnetar SGR (PSR) J1745–2900 ($\mu\simeq 1.6\times 10^{32}\ \mathrm{G\cdot cm^{3}}$ and $m\approx 1.5\ M_{\odot}$ [90]) orbiting around the SMBH Sgr A* ($M\simeq 3.8\times 10^{6}\ M_{\odot}$) can be calculated using observational data and can be approximately estimated as,

$$\beta=\frac{\mu_{\rm PSR\,J1745-2900}}{m_{\rm PSR\,J1745-2900}M_{\rm SgrA^{*}}}\approx 10.2. \tag{43}$$

The circular stable orbits of magnetized particles can also be defined by the standard conditions given in Eq. (24). Specific angular momentum and energy of the magnetized particle along the circular orbits can be expressed by the following expressions:

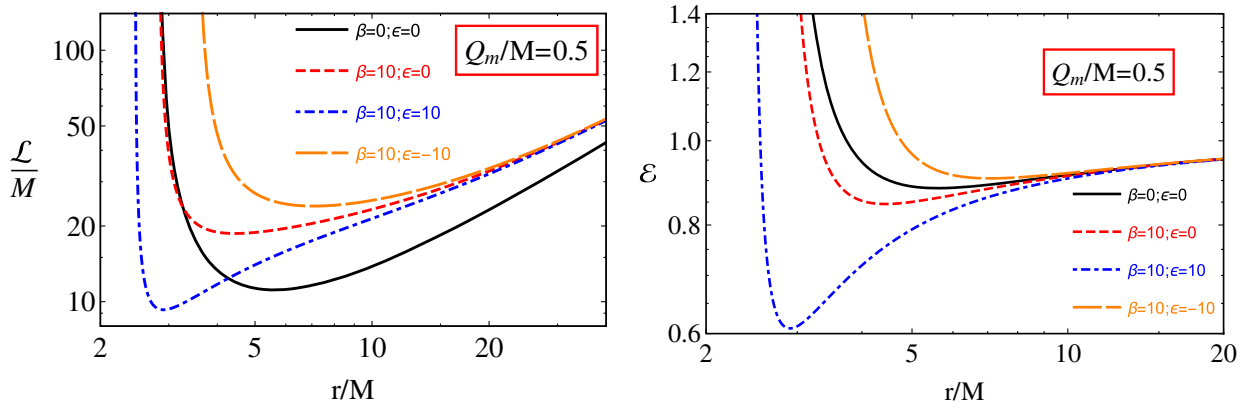

FIG. 16. Radial profiles of the specific angular momentum (top panel) and energy (bottom panel) of the magnetized particles around deformed magnetically charged RN BH in circular orbits for the different values of deformation parameter ϵ and for the fixed values of magnetic charge of the BH $Q_m/M = 0.5$ and the parameter $\beta = 10$ for the magnetar PSR J1745-2900 orbiting SgrA*.

$$\mathcal{L}^2 = \frac{r^5(r^2-\mathcal{B})}{2\mathcal{Z}}\left\{\frac{\epsilon M^3}{r^3}\left[\frac{9\mathcal{B}Q_m^2}{r^4}-\frac{16M\mathcal{B}}{r^3}+\frac{7\mathcal{B}-5Q_m^2}{r^2}+\frac{8M}{r}-3\right]+\frac{2M}{r}\left[1+\frac{2\mathcal{B}-Q_m^2}{Mr}-\frac{\mathcal{B}}{r^2}\left[5-\frac{3Q_m^2}{Mr}\right]\right]\right\},$$
$$\mathcal{E}^2 = \frac{2r}{\mathcal{Z}}\left(1+\epsilon\frac{M^3}{r^3}\right)^2\left[1-\frac{2M}{r}+\frac{Q_m^2}{r^2}\right]^2(r^4-\mathcal{B}^2). \tag{44}$$

Equation (44) is clear to see the effects of spacetime deformation and charge of the RN BH. By the reason we provide below graphical and numerical analysis.

Figure 16 demonstrates radial dependence of specific energy and angular momentum of magnetized particles around the deformed magnetically charged RN BH for different values of the deformation parameter and fixed values of the BH charge $Q_m/M = 0.5$ and the parameter $\beta = 10$ for the magnetar PSR J1745-2900 orbiting SgrA* treated as a magnetized particle. One can see from the figure that the existence of positive deformation of spacetime and magnetic dipole moment of magnetized particles lead to decrease both specific angular momentum and energy, while negative deformation acts in the oppositely.

Equation for ISCO radius can easily be found taking into account the standard conditions given in Eq. (24) and the effective potential provided in Eq. (41) in the following form:

$$\begin{aligned}&4r^6\{B^2[r^2(30M^2-21Mr+4r^2)+Q^2r(12r-37M)+12Q^4]+r^4[9MQ^2r+Mr^2(r-6M)-4Q^4]\}\\&+2M^3r^3\epsilon\{B^2[r^2(180M^2-132Mr+25r^2]+2Q^2r(39r-110M)+69Q^4)+r^4[6r^2(6M^2+Q^2)+60MQ^2r\\&+4Mr^3-25Q^4+3r^4]\}+2M^6\epsilon^2\{B^2[r^2(192M^2-162Mr+35r^2]+2Q^2r(45r-109M)+63Q^4)\\&+r^4[r^2(74Mr-96M^2-15r^2)+6Q^2(19M-7r)-35Q^4]\}\geq 0.\end{aligned} \tag{45}$$

One can notice that the form of Eq. (45) is quite complicated to solve with respect to the radial coordinate r which defines the ISCO radius. For this reason we prefer solve the Eq. (45) numerically and present the ISCO profiles in plot form.

Figure 17 demonstrates the dependence of ISCO radius of magnetized particles from the magnetic charge of the deformed RN BH (top panel) and deformation parameter (bottom panel) for the different values of the magnetic charge of the BH and deformation parameter at the fixed value of the parameter $\beta = 10$ (for the magnetar again). One can see from the first sight that ISCO radius decreases with increasing magnetic charge of pure RN BH (at $\epsilon = 0$) and the existence of magnetic dipole moment of magnetized particles lead to the decreasing to be "faster" due to magnetic interaction between the magnetic dipole moment of magnetized particle and magnetic charge of the BH. Moreover, the increase of positive (negative) spacetime deformation decreases (increases) the ISCO radius.

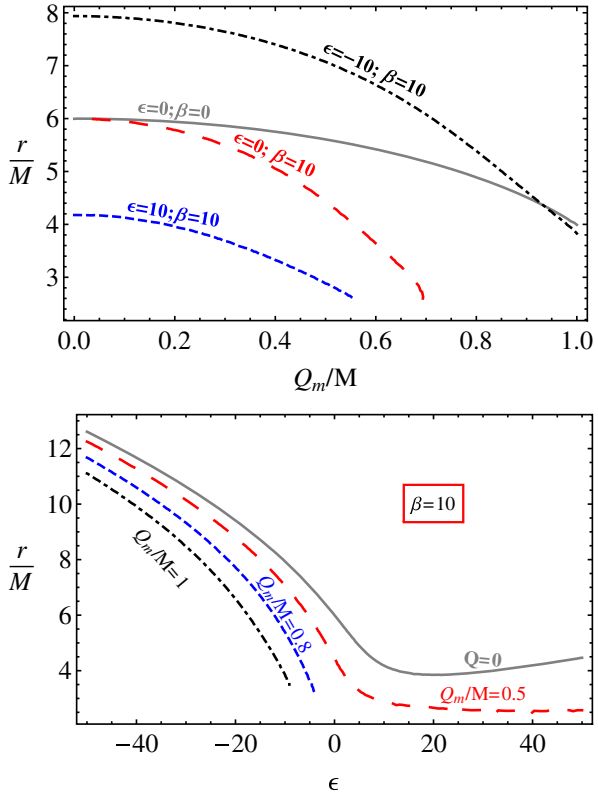

FIG. 17. ISCO radius of a magnetized particle around the deformed magnetically charged RN BHs as function of the magnetic charge (top panel) and deformation parameter (bottom panel) treating the magnetar PSR J1745-2900 orbiting SgrA* with parameter $\beta = 10$.

Now, here we provide comparisons of effects of deformed magnetically charged RN and Kerr BHs on ISCO radius of magnetized particles. Note that the magnetized particles can be considered as test neutral particles in the absence of external or/and proper magnetic field around Kerr BHs. Let us focus on showing the degeneracy between the magnetic charge of the deformed RN BH and the spin of rotating Kerr BH providing exactly the same values of ISCO radius for different values of the deformed RN BH.

Figure 18 illustrates relationship between degeneracy values of spin of the rotating Kerr BH and deformed magnetically charged RN BH providing the same values for ISCO radius of the magnetar orbiting SgrA* with the parameter $\beta = 10$ for different values of the deformation parameter. From the figure one can notice that by a detailed numerical analysis of ISCO radius of the magnetar with the parameter $\beta = 10$ that in pure RN BH case the magnetic charge of the BH is in the range $Q_m/M \in (0, 0.692)$. It mimics the spin parameter of the Kerr BH up to $a/M \simeq 0.8$. In the case when deformation parameter $\epsilon = 10$ the mimic values of the magnetic charge of the deformed RN BH and the spin of the Kerr BH providing the same value for ISCO radius of the magnetized particle with the parameter

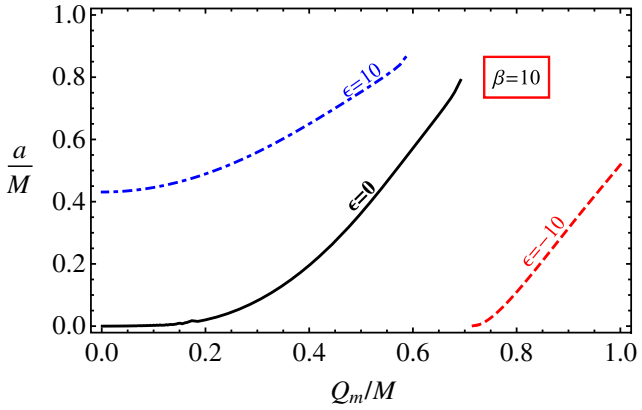

FIG. 18. Relation between degeneracy values of the spin parameter of rotating Kerr BH and magnetic charge of RN BH providing exactly the same values of ISCO radius for the fixed values of the parameter $\beta = 10$.

$\beta = 10$, takes the values in the range of $Q_m/M \in (0, 0.5856)$ and $a/M \in (0.415, 0.87)$, while in the case of the negative value of the deformation parameter $\epsilon = -10$, the degeneracy values $Q_m/M \in (0.71, 1)$ and $a/M \in (0.415, 0.527)$.

V. CONCLUSION

In this paper, we have first focused on the discussion of the dynamics of neutral particles around a deformed RN BH. The performed analysis of specific energy and angular momentum have shown that the increase of positive (negative) specetime deformation leads to decrease (increase) of the energy and angular momentum. The minimum value of radius for circular orbits decreases with increase in both positive deformation parameter and the BH charge, while it increases in the presence of negative spacetime deformation. From the study of ISCO, we find that ISCO radius reaches its minimum value ($r_{\rm isco}/M = 3.8564$) at the deformation parameter $\epsilon = 20.4547$ in the Schwarzschild spacetime $Q = 0$. In the extreme charged RN case, the ISCO radius reaches its minimum at $\epsilon = 6.1741$ taking the value $r_{\rm isco}/M = 2.2665$.

In addition, the static deformed RN BH reflects the effects of rotating Kerr BH providing exactly the same ISCO radius for the test neutral particles. Taking into account that pure RN BH charge can mimic spin of rotating Kerr BH up to $a/M \simeq 0.48$, it implies that the gravitational effects of the spin of supermassive RN BH SgrA* is equivalent to the charge $Q/M \simeq 0.83$. The charge of the deformed RN BH with deformation parameter $\epsilon = 6.1741$ can mimic the BH spin parameter up to $a/M \approx 0.88$. It confirms that effect of a charge of RN BH cannot cover the effects of the spin of SMBH M87 which is estimated as $a/M = 0.9 \pm 0.05$ [91].

Similar effects of spacetime deformation have also been discussed in the study of energy efficiency from accretion

to the deformed RN BH together with its charge. The maximum efficiency ($\widetilde{13}.4\%$) may occur at $\epsilon = 32$ for Schwarzchild BH, while for extremely charged RN BH it reaches up to 20.02% with the spacetime deformation $\epsilon = 9.07$.

In the second part of the paper, we have explored motion of electrically charged particles around electrically charged deformed RN BH. It is found that there are two solutions for the square of the specific angular momentum for circular motion of electrically charged particles, which are due to symmetry with respect to the replacement of $qQ \to -qQ$ being responsible for the nature of the Coulomb interaction. It is observed that the ISCO radius rapidly increases with increasing RN BH charge in the case of attractive interaction($qQ < 0$) while it decreases with respect to increase in charge of RN BH for the repulsive Coulomb interaction ($qQ > 0$). There is a critical value for the BH charge where ISCO radius goes to infinity due to strong attractive Coulomb force and the critical value marginally increases (decreases) with the increase of spacetime deformation due to the dominating behavior of the electric forces. Analysis of the effects of spectime deformation on ISCO radius have shown that the effect becomes stronger for large values of the BH charge. Moreover, it is found that electrically charged particle can be orbiting in the same ISCO radius around the deformed RN BH with two values of the deformation parameter for $Q < Q_{\rm crit}$ ($qQ < 0$).

Finally, we have also thoroughly studied the magnetized particle's motion around deformed magnetically charged RN BH, treating the magnetar SGR (PSR) J1745-2900 (orbiting SMBH SgrA*) as a magnetized particle. It is shown that increasing the magnetic charge of the deformed RN BH, ISCO radius of magnetized particle decreases faster than that of the neutral particle. The detailed comparison of the effects of magnetic charge of deformed RN BH with that of the spin of the rotating Kerr BH have shown that for pure RN BH spacetime the magnetic charge of the BH [being in the range $Q_m/M \in (0, 0.692)$] can mimic the spin parameter of the Kerr BH up to $a/M \simeq 0.812$. In cases when deformation parameter $\epsilon = 10$ and $\epsilon = -10$, the mimic values of the magnetic charge of the deformed RN BH and the spin of the Kerr BH lies between the ranges $Q_m/M \in (0, 0.5856)$; $a/M \in (0.415, 0.87)$ and $Q_m/M \in (0.71, 1)$; $a/M \in (0, 0.527)$, respectively. The obtained results on the influence of the magnetic interaction on the ISCO orbits shows that the observed degeneracy between magnetic and BH parameters (being responsible for strong gravitational field) are significant candidate problems for a future study regarding measurement of the electromagnetic field by the alternate methods. It is hoped that this will possibly explain how the effects of the gravitational field can be extracted and an understanding of gravity theories in the strong field regime can be achieved.

ACKNOWLEDGMENTS

Ashfaque H. Bokhari at KFUPM and Bobomurat Ahmedov would like to acknowledge the support received from KFUPM under University Funded Grant No. SB191039. This research is supported also by Grants No. VA-FA-F-2-008 and No. MRB-AN-2019-29 of the Ministry of Innovative Development of the Republic of Uzbekistan.

[1] H. Reissner, Ann. Phys. (Berlin) **355**, 106 (1916).
[2] G. Nordström, K. Ned. Akad. Wet. Proc. Ser. B Phys. Sci. **20**, 1238 (1918), https://ui.adsabs.harvard.edu/abs/1918KNAB...20.1238N/abstract.
[3] J. Bardeen, in *Proceedings of GR5*, edited by C. DeWitt and B. DeWitt (Gordon and Breach, Tbilisi, USSR, 1968), p. 174.
[4] E. Ayón-Beato and A. García, Phys. Rev. Lett. **80**, 5056 (1998).
[5] E. Ayon-Beato, Phys. Lett. B **464**, 25 (1999).
[6] A. Wang and R. Maartens, Phys. Rev. D **81**, 024009 (2010).
[7] B. Toshmatov, Z. Stuchlík, J. Schee, and B. Ahmedov, Phys. Rev. D **97**, 084058 (2018).
[8] T. Johannsen and D. Psaltis, Astrophys. J. **716**, 187 (2010).
[9] T. Johannsen and D. Psaltis, Phys. Rev. D **83**, 124015 (2011).
[10] L. Rezzolla and A. Zhidenko, Phys. Rev. D **90**, 084009 (2014).
[11] N. Yunes and F. Pretorius, Phys. Rev. D **80**, 122003 (2009).
[12] F. Atamurotov, A. Abdujabbarov, and B. Ahmedov, Phys. Rev. D **88**, 064004 (2013).
[13] A. Hakimov and F. Atamurotov, Astrophys. Space Sci. **361**, 112 (2016).
[14] J. R. Rayimbaev, B. J. Ahmedov, N. B. Juraeva, and A. S. Rakhmatov, Astrophys. Space Sci. **356**, 301 (2015).
[15] J. Rayimbaev, B. Turimov, F. Marcos, S. Palvanov, and A. Rakhmatov, Mod. Phys. Lett. A **35**, 2050056 (2020).
[16] C. Liu, S. Chen, and J. Jing, Astrophys. J. **751**, 148 (2012).
[17] J. Jiang, C. Bambi, and J. F. Steiner, J. Cosmol. Astropart. Phys. 05 (2015) 025.
[18] D. Liu, Z. Li, and C. Bambi, J. Cosmol. Astropart. Phys. 01 (2015) 020.
[19] C. Bambi, J. Cosmol. Astropart. Phys. 08 (2013) 055.
[20] C. Bambi, Astrophys. J. **761**, 174 (2012).
[21] B. P. Abbott, R. Abbott, T. D. Abbott, M. R. Abernathy, F. Acernese, K. Ackley, C. Adams, T. Adams, P. Addesso, R. X. Adhikari *et al.*, Phys. Rev. Lett. **116**, 061102 (2016).

[22] LIGO Scientific and Virgo Collaborations, arXiv:1602.03841.
[23] B. P. Abbott, R. Abbott, T. D. Abbott, M. R. Abernathy, F. Acernese, K. Ackley, C. Adams, T. Adams, P. Addesso, R. X. Adhikari *et al.*, Phys. Rev. Lett. **116**, 221101 (2016).
[24] K. Akiyama *et al.* (Event Horizon Telescope Collaboration), Astrophys. J. **875**, L1 (2019).
[25] K. Akiyama *et al.* (Event Horizon Telescope Collaboration), Astrophys. J. **875**, L6 (2019).
[26] R. Abuter *et al.*, Astron. Astrophys. **618**, L10 (2018).
[27] R. Abuter *et al.* (Gravity Collaboration), Astron. Astrophys. **615**, L15 (2018).
[28] A. A. Tursunov and M. Kološ, Phys. At. Nucl. **81**, 279 (2018).
[29] D. Pugliese, H. Quevedo, and R. Ruffini, arXiv:1003.2687.
[30] D. Pugliese, H. Quevedo, and R. Ruffini, Phys. Rev. D **83**, 104052 (2011).
[31] J. Rayimbaev, M. Figueroa, Z. c. v. Stuchlík, and B. Juraev, Phys. Rev. D **101**, 104045 (2020).
[32] B. Turimov, J. Rayimbaev, A. Abdujabbarov, B. Ahmedov, and Z. c. v. Stuchlík, Phys. Rev. D **102**, 064052 (2020).
[33] N. A. Sharp, Gen. Relativ. Gravit. **10**, 659 (1979).
[34] V. P. Frolov and I. D. Novikov, *Black Hole Physics, Basic Concepts and New Developments*, Frolov98 (Kluwer Academic Publishers, Dordrecth, Netherlands, 1998).
[35] A. Jawad, F. Ali, M. Jamil, and U. Debnath, Commun. Theor. Phys. **66**, 509 (2016).
[36] S. Hussain and M. Jamil, Phys. Rev. D **92**, 043008 (2015).
[37] M. Jamil, S. Hussain, and B. Majeed, Eur. Phys. J. C **75**, 24 (2015).
[38] S. Hussain, I. Hussain, and M. Jamil, Eur. Phys. J. C **74**, 3210 (2014).
[39] G. Z. Babar, M. Jamil, and Y.-K. Lim, Int. J. Mod. Phys. D **25**, 1650024 (2016).
[40] M. Bañados, J. Silk, and S. M. West, Phys. Rev. Lett. **103**, 111102 (2009).
[41] B. Majeed and M. Jamil, Int. J. Mod. Phys. D **26**, 1741017 (2017).
[42] A. Zakria and M. Jamil, J. High Energy Phys. 05 (2015) 147.
[43] I. Brevik and M. Jamil, Int. J. Geom. Methods Mod. Phys. **16**, 1950030 (2019).
[44] M. De Laurentis, Z. Younsi, O. Porth, Y. Mizuno, and L. Rezzolla, Phys. Rev. D **97**, 104024 (2018).
[45] B. Narzilloev, A. Abdujabbarov, C. Bambi, and B. Ahmedov, Phys. Rev. D **99**, 104009 (2019).
[46] B. Narzilloev, J. Rayimbaev, A. Abdujabbarov, and C. Bambi, arXiv:2005.04752.
[47] B. Narzilloev, J. Rayimbaev, S. Shaymatov, A. Abdujabbarov, B. Ahmedov, and C. Bambi, Phys. Rev. D **102**, 044013 (2020).
[48] V. S. Morozova, L. Rezzolla, and B. J. Ahmedov, Phys. Rev. D **89**, 104030 (2014).
[49] J. Rayimbaev, B. Turimov, and B. Ahmedov, Int. J. Mod. Phys. D **28**, 1950128 (2019).
[50] B. Turimov, B. Ahmedov, M. Kološ, and Z. Stuchlík, Phys. Rev. D **98**, 084039 (2018).
[51] A. Tursunov, Z. Stuchlík, and M. Kološ, Phys. Rev. D **93**, 084012 (2016).
[52] A. A. Abdujabbarov, B. J. Ahmedov, and N. B. Jurayeva, Phys. Rev. D **87**, 064042 (2013).
[53] Z. Stuchlík, M. Kološ, J. Kovář, P. Slaný, and A. Tursunov, Universe **6**, 26 (2020).
[54] B. Turimov, Int. J. Mod. Phys. D **27**, 1850092 (2018).
[55] F. de Felice and F. Sorge, Classical Quantum Gravity **20**, 469 (2003).
[56] B. Toshmatov, A. Abdujabbarov, B. Ahmedov, and Z. Stuchlík, Astrophys Space Sci **360**, 19 (2015).
[57] J. R. Rayimbaev, Astrophys. Space Sci. **361**, 288 (2016).
[58] O. G. Rahimov, Mod. Phys. Lett. A **26**, 399 (2011).
[59] O. G. Rahimov, A. A. Abdujabbarov, and B. J. Ahmedov, Astrophys. Space Sci. **335**, 499 (2011).
[60] K. Haydarov, A. Abdujabbarov, J. Rayimbaev, and B. Ahmedov, Universe **6**, 44 (2020).
[61] K. Haydarov, J. Rayimbaev, A. Abdujabbarov, and S. Palvanov, and D. Begmatova, Eur. Phys. J. C **80**, 399 (2020).
[62] J. Vrba, A. Abdujabbarov, M. Kološ, B. Ahmedov, Z. c. v. Stuchlík, and J. Rayimbaev, Phys. Rev. D **101**, 124039 (2020).
[63] A. Abdujabbarov, J. Rayimbaev, B. Turimov, and F. Atamurotov, Phys. Dark Universe **30**, 100715 (2020).
[64] J. Rayimbaev, A. Abdujabbarov, M. Jamil, and W. Han, arXiv:2009.04898.
[65] B. Toshmatov and D. Malafarina, Phys. Rev. D **100**, 104052 (2019).
[66] A. Papapetrou, in *Nonlinear Gravitodynamics: The Lense-Thirring Effect*, edited by R. Remo and S. Costantino (World Scientific, Singapore, 2003), pp. 393–403.
[67] W. G. Dixon, Proc. R. Soc. A **314**, 499 (1970).
[68] B. Toshmatov, O. Rahimov, B. Ahmedov, and D. Malafarina, Eur. Phys. J. C **80**, 675 (2020).
[69] A. Tursunov, M. Zajaček, A. Eckart, M. Kološ, S. Britzen, Z. Stuchlík, B. Czerny, and V. Karas, Astrophys. J. **897**, 99 (2020).
[70] C. Bambi, J. Cosmol. Astropart. Phys. 05 (2011) 009.
[71] S. Gillessen, F. Eisenhauer, T. K. Fritz, H. Bartko, K. Dodds-Eden, O. Pfuhl, T. Ott, and R. Genzel, Astrophys. J. Lett. **707**, L114 (2009).
[72] J. Rayimbaev, A. Abdujabbarov, M. Jamil, B. Ahmedov, and W.-B. Han, Phys. Rev. D **102**, 084016 (2020).
[73] B. Narzilloev, J. Rayimbaev, S. Shaymatov, A. Abdujabbarov, B. Ahmedov, and C. Bambi, Phys. Rev. D **102**, 104062 (2020).
[74] J. Rayimbaev and P. Tadjimuratov, Phys. Rev. D **102**, 024019 (2020).
[75] A. Abdujabbarov, J. Rayimbaev, F. Atamurotov, and B. Ahmedov, Galaxies **8**, 76 (2020).
[76] J. Rayimbaev, P. Tadjimuratov, A. Abdujabbarov, B. Ahmedov, and M. Khudoyberdieva, arXiv:2010.12863.
[77] B. Narzilloev, J. Rayimbaev, S. Shaymatov, A. Abdujabbarov, B. Ahmedov, and C. Bambi, Phys. Rev. D **102**, 044013 (2020).
[78] R. Rahim and K. Saifullah, Ann. Phys. (Amsterdam) **405**, 220 (2019).
[79] C. M. Will, Living Rev. Relativity **9**, 3 (2006).
[80] J. M. Bardeen, W. H. Press, and S. A. Teukolsky, Astrophys. J. **178**, 347 (1972).
[81] M. Zajaček, A. Tursunov, A. Eckart, and S. Britzen, Mon. Not. R. Astron. Soc. **480**, 4408 (2018).
[82] M. Zajacek and A. Tursunov, Observatory **139**, 231 (2019), https://ui.adsabs.harvard.edu/abs/2019Obs...139..231Z/abstract.

[83] I. D. Novikov and K. S. Thorne, in *Black Holes (Les Astres Occlus)*, edited by C. Dewitt and B. S. Dewitt (Gordon & Breach, New York, 1973), pp. 343–450.
[84] W.-H. Bian and Y.-H. Zhao, Publ. Astron. Soc. Jpn. **55**, 599 (2003).
[85] A. Tripathi, S. Nampalliwar, A. B. Abdikamalov, D. Ayzenberg, C. Bambi, T. Dauser, J. A. García, and A. Marinucci, Astrophys. J. **875**, 56 (2019).
[86] A. B. Abdikamalov, D. Ayzenberg, C. Bambi, S. Nampalliwar, A. Tripathi, J. Wong, Y. Xu, J. Yan, Y. Yan, and Y. Yang, MDPI Proc. **17**, 2 (2019).
[87] A. B. Abdikamalov, D. Ayzenberg, C. Bambi, T. Dauser, J. A. Garcia, S. Nampalliwar, A. Tripathi, and M. Zhou, Astrophys. J. **899**, 80 (2020).
[88] A. Cardenas-Avendano, M. Zhou, and C. Bambi, Phys. Rev. D **101**, 123014 (2020).
[89] M. Zhou, A. B. Abdikamalov, D. Ayzenberg, C. Bambi, V. Grinberg, and A. Tripathi, Mon. Not. R. Astron. Soc. **496**, 497 (2020).
[90] K. Mori *et al.*, Astron. J. Lett. **770**, L23 (2013).
[91] F. Tamburini, B. Thidé, and M. Della Valle, Mon. Not. R. Astron. Soc. **492**, L22 (2020).